JOM, Vol. 76, No. 2, 2024
https://doi.org/10.1007/s11837-023-06271-x

Realizing the Ultrafast Homogenization of Bearing Steel Based on Solute Atom Diffusion Under Pulsed Electric Current

ZHONGXUE WANG,[1,4] DANDAN ZHANG,[2] JIANQIAO HAO,[3] LI WANG,[4] MENGCHENG ZHOU,[1,5] and XINFANG ZHANG[1,6]

1.—School of Metallurgical and Ecological Engineering, University of Science and Technology Beijing, Beijing 100083, People's Republic of China. 2.—School of Physics and Optoelectronic Engineering, Ludong University, Yantai 264025, People's Republic of China. 3.—Research Institute of Technology, Shougang Group Co., Ltd., Beijing 100043, People's Republic of China. 4.—Research Institute of Shandong Iron and Steel Group Co. Ltd., Jinan 271105, People's Republic of China. 5.—e-mail: 309265645@qq.com. 6.—e-mail: xfzhang@ustb.edu.cn

Due to the miscibility gap between phases in bearing steel, severe elemental segregation will occur in the solidified structure, and many liquation carbides are precipitated between dendrites, which will significantly reduce the subsequent processing deformation ability of materials. In this study, when a pulsed electric current is applied to the sample, the additional electrical free energy generated under the electromagnetic interaction significantly changes the thermodynamic state of the system. The liquation carbide and element segregation can be eliminated at a relatively lower temperature (1100°C), and the homogenization effect is equivalent to that of industrial homogenization treatment (1220°C). The pulsed electric current significantly improves the atomic diffusion rate and shortens the homogenization treatment time (the industrial homogenization treatment under the thermal field is about 300 min, and the pulsed electric current treatment is about 30 min). In addition, due to the reduction of the treatment temperature and the shortening of the treatment time, the pulsed electric current treatment effectively inhibits the rapid growth of the grain size after the homogenization of the slab, which provides a good initial fine grain structure for the subsequent hot deformation treatment (such as rolling and forging), and significantly improves the quality of the slab.

INTRODUCTION

Bearing steel is one of the most demanding special steels in iron and steel production. It is usually used to manufacture precision parts of bearing instruments, molds, and machines.[1] High-end bearing steel has extremely strict requirements for comprehensive mechanical properties, such as extremely high strength, hardness, wear resistance, and contact fatigue life. In the production and preparation process, high requirements are put forward for each process to obtain appropriate structures, compositions, and homogenization.[2–5] In order to improve the comprehensive mechanical properties of bearing steel, it is necessary to add a large amount of C, Cr, Mn, and other alloy elements into the material. However, the addition of such elements leads to the formation of heterogeneous microstructures in the steel during solidification: i.e., the dendrite segregation will be formed in the solidification structure due to the miscibility gap between phases, while the solidification end of the bearing steel, the element segregation in the molten steel is further intensified, and, finally, large pieces of carbides, namely liquation carbide, are formed by eutectic reaction. The formation of heterogeneous structures leads to a significant reduction of material plasticity, which seriously damages the machinability of the materials.[6]

(Received April 26, 2023; accepted October 25, 2023; published online November 9, 2023)

To solve the problem of segregation during solidification, it is necessary to conduct high-temperature homogenization annealing treatment before thermal deformation treatment.[4,7] Dendrite segregation and harmful liquation carbide can be eliminated with element diffusion during homogenization treatment.[8] To ensure the homogenization effect in bearing steel, the traditional homogenization annealing process requires to be held at a high temperature for a long time. The industrial homogenization temperature is generally 1220°C, and the holding time is not less than 300 min.[4] Thus, traditional homogenization annealing has high production costs and low production efficiency, while cast grain is easy to grow when bearing steel is kept at high temperature for a long time.[9] Too coarse a grain structure will significantly reduce the hot workability of materials. Therefore, it is of great significance to effectively reduce the homogenization annealing temperature, shorten the homogenization annealing time, and improve the homogenization structure. Since the last century, extensive research has been carried out on the segregation behavior of elements in the solidification process of bearing steel and the diffusion behavior of atoms in the homogenization process.[10–12] The solidification structure of bearing steel can be improved, and the homogenization treatment time can be shortened, by upgrading the smelting process and adjusting the alloy composition.[13,14] According to the element composition and evolution law of liquation carbide in GCr15 bearing steel, the homogenization annealing process of the steel was optimized, which improved the homogenization quality and production efficiency.[15,16] However, the above research was all optimized and improved on the basis of traditional heat treatment, and the homogenization process was not effectively shortened, and the grain coarsening problem was not completely solved. In addition, additional processes such as alloying further complicate the production process of bearing steel and increase the cost.

With the development of bearing steel towards large-scale and multi-alloying, more stringent requirements are put forward for the quality of the steel.[17,18] As a new external field processing method, pulsed electric current processing has many advantages, such as high efficiency and low energy consumption.[19,20] When the current passes through the metal, the athermal effect formed by the interaction of electrons and atoms will significantly reduce the thermodynamic energy barrier of phase transition.[21] At the same time, the high-speed moving drift electrons can significantly enhance the mobility of the atoms, improve their diffusion rate, and effectively shorten the treatment time.[22] For the second-phase particles formed due to element segregation in materials, researchers have conducted much research on the evolution behavior of the particles under a pulsed electric current, such as harmful hydrides formed by the interaction of titanium and hydrogen, G phase in two-phase stainless steel, η phase, and low melting point eutectic, etc.[23–26] In a short time, the pulsed electric current can effectively control the microstructure of the material and dissolve the second-phase particles at a lower temperature. The essential question of homogenization annealing in bearing steel is to eliminate dendritic segregation and harmful liquid carbide. The above achievements provide a theoretical basis for the application of pulsed electric current technology in homogenization treatment of as-cast bearing steel, and provide a new idea for shortening the homogenization annealing time and optimize the annealing process in industry.

In view of the above problems, in this study a pulsed electric current was applied to as-cast GCr15 bearing steel. Combined with the characteristic structure and distribution state of the heterogeneous components, the differential distribution of the micro-area physical field under the current was analyzed, and the dissolution mechanism of the liquidus carbide and dendrite in the process of pulse current-controlled homogenization is studied.

EXPERIMENTAL

The raw material was as-cast GCr15 bearing steel with the chemical composition in weight percent of 1% C, 1.57% Cr, 0.35% Mn, 0.25% Si, 0.02% P, and 0.02% S. Several 50 mm × 10 mm × 1.5 mm samples were cut from the core of the slab. Before the pulsed treatment, the sample surface was polished with 2000-mesh sandpaper to ensure good contact between the sample and the electrode, to avoid an abnormal temperature rise of the sample due to Joule heat generated by excessive local resistance. The pulsed electric current treatment was carried out by a pulse generator and the electropulsing parameters are listed in Table I (E1, E2, E3). A K-type thermocouple was welded to the center of the sample surface to measure the temperature rise of the samples, and the samples for comparison were annealed at the same temperature and time. The heat treatment parameters are listed in Table I (H1, H2, H3). The thermal contrast treatment was carried out in a tubular furnace. In addition, the temperature rate of the thermal contrast sample should be consistent with that of the pulsed sample to avoid the influence of temperature rates on the experimental results. In order to prevent oxidation and decarburization of the samples, the heating was carried out in argon atmosphere. Additionally, the as-cast bearing steel sample (Sample G1) was homogenized at 1220°C for 300 min and then air-cooled to room temperature, referring to the current industrial production process and other research results.[27,28]

The processed samples were ground with SiC sandpaper and polished with a diamond solution, then etched with a solution of anhydrous ethanol

Table I. The parameters for treatment of the GCr15 bearing steel

No.	Frequency (kHz)	Current density (A/mm^2)	Processing time (min)	Processing temperature (°C)
E1	31.6	14.7	30	900
E2	31.6	17.2	30	1000
E3	31.6	19.4	30	1100
H1	0	0	30	900
H2	0	0	30	1000
H3	0	0	30	1100

containing 4% nitric acid for 30 s. The microstructures of the samples were analyzed by an optical metallurgical microscope (OM; DM5000X; UOP) and a scanning electron microscope (SEM; JSM 6701F; JEOL). Simultaneously, the original ingot sample (Y-1) was jet-electropolished in a 10% perchloric acid and 90% ethanol solution at − 25°C. The structure of the liquation carbide was analyzed by a transmission electron microscope (TEM; Tecnai F30; FEI). A field-emission electron probe microanalyzer (EPMA; 1720 Series; SHIMADZU) was employed to investigate the element concentration and distribution on the samples with the different treatment processes. The pulsed sample (E3) and industrial long process-annealed sample (G1) were selected to further analyze the effect of different treatments on grain size. After grinding and polishing, the original austenite grain boundary was corroded with supersaturated picric acid solution + 1 g sodium dodecyl benzene sulfonate at 75°C for 30 s.

When a high-frequency current passes through the conductor, the skin effect forces the current to pass only along the surface of the conductor. Considering the high current frequency (31.6 kHz) in this study, the skin depth[29] was calculated to be about 2.8 mm, and the thickness of the sample was only 1.5 mm, so the influence of the skin effect during this study can be ignored.

RESULTS AND DISCUSSION

Solidification Structure of Bearing Steel

Figure 1 shows the microstructure of the bearing steel after solidification, and obvious dendrite segregation can be observed. The black region could be described as an island or background structure that harbors dendrites connected to one another to form grain boundaries, usually called the dendritic core, and the white region is interdendritic (Fig. 1a. Quantitative analysis of the dendrites was carried out with ImageJ software. The results show that the area of dendrites under the two-dimensional plane accounts for about 3.7% and the dendrite spacing is about 109.5 μm. Meanwhile, some shrinkage defects were observed in Fig. 1b, which is related to the element segregation in the local region.[30] In order to avoid the impact of shrinkage on the results, the samples used in this study avoided these areas. A large number of precipitates, namely, liquation carbide, formed in the interdendritic region. Irregular massive liquation carbide can be observed under the two-dimensional plane, and the edge of the carbide extends outwards as a needle (Fig. 1c). Liquation carbide is also known as eutectic carbide or primary cementite, while the three-dimensional morphology of the liquation carbide is irregular lamellar,[12] which is consistent with what was observed in Fig. 1d. When the lamellar is relatively dense, the lamellar spacing is very small and the morphology of the liquation carbide in the two-dimensional plane is irregular blocky. When the lamellar distribution is relatively loose, the lamellar spacing is large, and the morphology under the two-dimensional plane is needle-like. Figure 1e shows a bright-field TEM image of the liquation carbide, and the identification of the selected area electron diffraction pattern confirmed that it is liquation carbide with an orthogonal crystal structure (θ-Fe_3C). The liquation carbide is a brittle and harmful phase, which significantly deteriorates the hot workability of bearing steel. The residual liquation carbide particles will also affect the service life of the final bearing products.

In addition, a certain number of dark black particles were observed in the interior and surrounding regions of some liquation carbides. Figure 2 shows the element plane distribution results by energy dispersive spectroscopy (EDS). It can be seen that Cr and Mn are obviously enriched in the liquation carbide, and that the content of Fe is lower than that of the matrix.

Pulsed Electric Current Reducing the Dissolution Temperature of Liquation Carbide

When the pulsed sample temperature was 900°C, a large amount of liquation carbide was dissolved (Fig. 3a). With the increase of the pulsed treatment temperature, the liquation carbides were further dissolved, and only a small number of residual particles of liquation carbide were observed in local areas in the pulsed sample under 1000°C (Fig. 3c). The liquation carbide has been completely dissolved in the pulsed sample under 1100°C, and a martensite structure was formed during cooling of the treated sample (Fig. 3e). By analyzing the thermal contrast sample, it was found that, when the sample

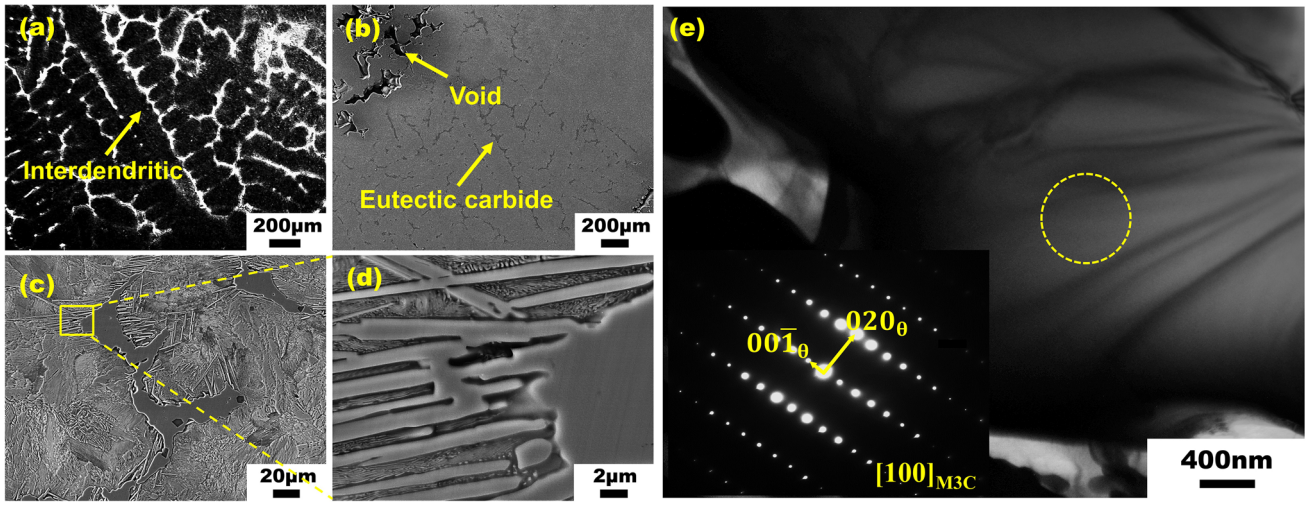

Fig. 1. Microstructure of as-cast bearing steel samples: (a) OM micrographs of the original ingot sample, (b, c) SEM of as-cast bearing steel samples, (d) the enlargement of the local area in (c), (e) bright-field TEM of the liquation carbide, selected area electron diffraction results of liquation carbide (the part circled), [100] θ-Fe_3C.

temperature was 900°C, the morphology of the liquation carbide shows no obvious change compared with the original sample (Fig. 1c). With the increase of the heat-treatment temperature, the carbides gradually dissolved, but the dissolution process of the carbides in the thermal field lagged significantly behind that of the samples treated with the pulsed electric current. Residual liquation carbide particles can even still be observed in the annealed sample at 1100°C.

The above results show that, compared with traditional homogenization annealing, the pulsed treatment can significantly dissolve interdendritic liquation carbide. Under high current density (19.4 A/m^2), the effect of the pulsed electric current is more significant, that is, at a relatively low treatment temperature (1100°C), the pulsed treatment can effectively eliminate segregation and achieve complete homogenization. More significantly, compared with the industrial homogenization treatment (300 min), the pulsed treatment time is only 30 min, which greatly shortens the homogenization annealing time.

The element segregation behavior of the bearing steel during solidification was calculated by the JMatPro software solidification module. Figure 4 shows the mass percentage change of the Cr, Mn, Si, and C elements in the residual liquid phase during the solidification of the bearing steel. Cr, Mn, Si, and C are all positive segregation elements, and, among them, the segregation of the C and Cr elements are the most serious, and the concentration in the residual liquid phase increases significantly with the solidification. Cr is the main forming element of liquation carbide (Fig. 2), and the enrichment of elements such as C and Cr at the solidification end in the residual liquid phase significantly promotes the precipitation of liquation carbide. As shown in Fig. 4b, the theoretical value of the precipitation temperature of liquation carbide in GCr15 bearing steel is about 1149°C.

Under a single thermal field, the dissolution of liquation carbide needs to meet certain thermodynamic conditions, that is, the treatment temperature needs to reach its solution temperature (1149°C). However, when the current passes through the sample, it will not only generate Joule heat but also generate additional electrical free energy in the system. Compared with the system in the same state (microstructure, temperature, pressure, etc.), the formation of electrical free energy will significantly change the dissolution behavior of precipitates.[31] The change of electrical free energy in the current carrying system can be expressed as:[32]

$$\Delta G_{\text{elec}} = kVj^2 \cdot \frac{\sigma_{\text{matrix}} - \sigma_{\text{carbide}}}{2\sigma_{\text{matrix}} + \sigma_{\text{carbide}}} \quad (1)$$

where ρ is the electrical resistivity (the measured value is about 2.16×10^{-7} Ω m), f is the current frequency, u_0 is the vacuum permeability (the measured value is about $4\pi \times 10^{-7}$ N/A^2), u_r is the relative permeability (the measured value is about 300), σ_{matrix} and σ_{carbide} are the conductivity of the matrix and the liquation carbide (Fe_3C) respectively, V is the volume, j is the current density, and k is a geometric factor related to the morphology and location of the precipitated phase. Matthiessen's rule shows that the resistivity increases with the solute concentration of the atom. Compared with the matrix (γ-Fe), the precipitated phase (liquation carbide) has more solute atoms and a stronger electron scattering effect. Therefore, the conductivity of the precipitated phase is lower than that of the matrix, i.e., $\sigma_{\text{matrix}} > \sigma_{\text{carbide}}$, $\Delta G_{\text{elec}} > 0$. ΔG_{elec} is directly related to the geometric factor, k, if the liquation carbide dissolves (k value changes), the conductivity difference between the liquation

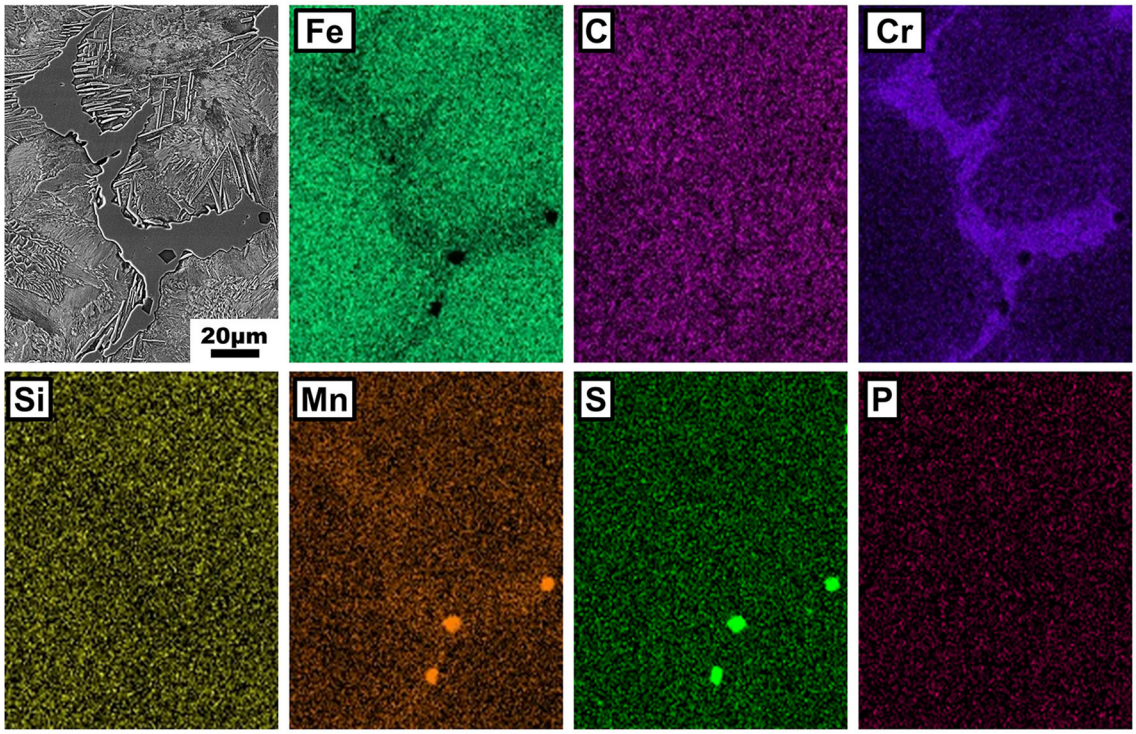

Element	Atomicity	Quality (%)	Normalized quality (%)	Atom (%)
Fe	26	75.25	81.95	58.92
C	6	8.27	9.01	30.12
Cr	24	3.92	4.27	3.30
Si	14	0.09	0.10	0.14
Mn	25	1.98	2.15	1.57
S	16	0.19	0.21	0.26
P	15	0.05	0.06	0.07

Fig. 2. EDS element distribution of liquation carbide and surrounding regions.

carbide and the matrix will gradually decrease. The electrical free energy will evolve along the decreasing direction to meet the requirements of reducing the free energy in the whole system. In essence, it is the additional electrical free energy, ΔG_{elec}, that changes the system energy, and thus the dissolution behavior takes place at relatively low temperature.

Dissolution Process of Liquation Carbide Under Pulsed Electric Current

Compared with the traditional heat treatment, the pulsed electric current significantly promoted the dissolution of the liquation carbide. In order to "capture" the intermediate state of liquation carbide dissolution under the pulsed electric current, the current treatment experiments lasting for different times (10 min, 20 min, 30 min) under this condition (E2: 1000°C-31.6 kHz-10.9 A/mm^2) were performed. As shown in Fig. 5, after 10 min of pulsed treatment, the lamellae of the liquation carbide were partially dissolved, the lamellar spacing was significantly expanded, and the morphology of the liquation carbide was decomposed from a compact block to loose needle. With the increase of treatment time, the lamellar spacing gradually increased, and the massive liquation carbides have basically disappeared at 20 min. After further prolonging the treatment time, the lamellae of the liquation carbide further broke down and decomposed. Up to 30 min, the morphology of the remaining liquation carbide was irregular small particles.

The current significantly promoted the dissolution of the liquation carbide, and the liquation carbide rapidly decomposed into needle-shaped and

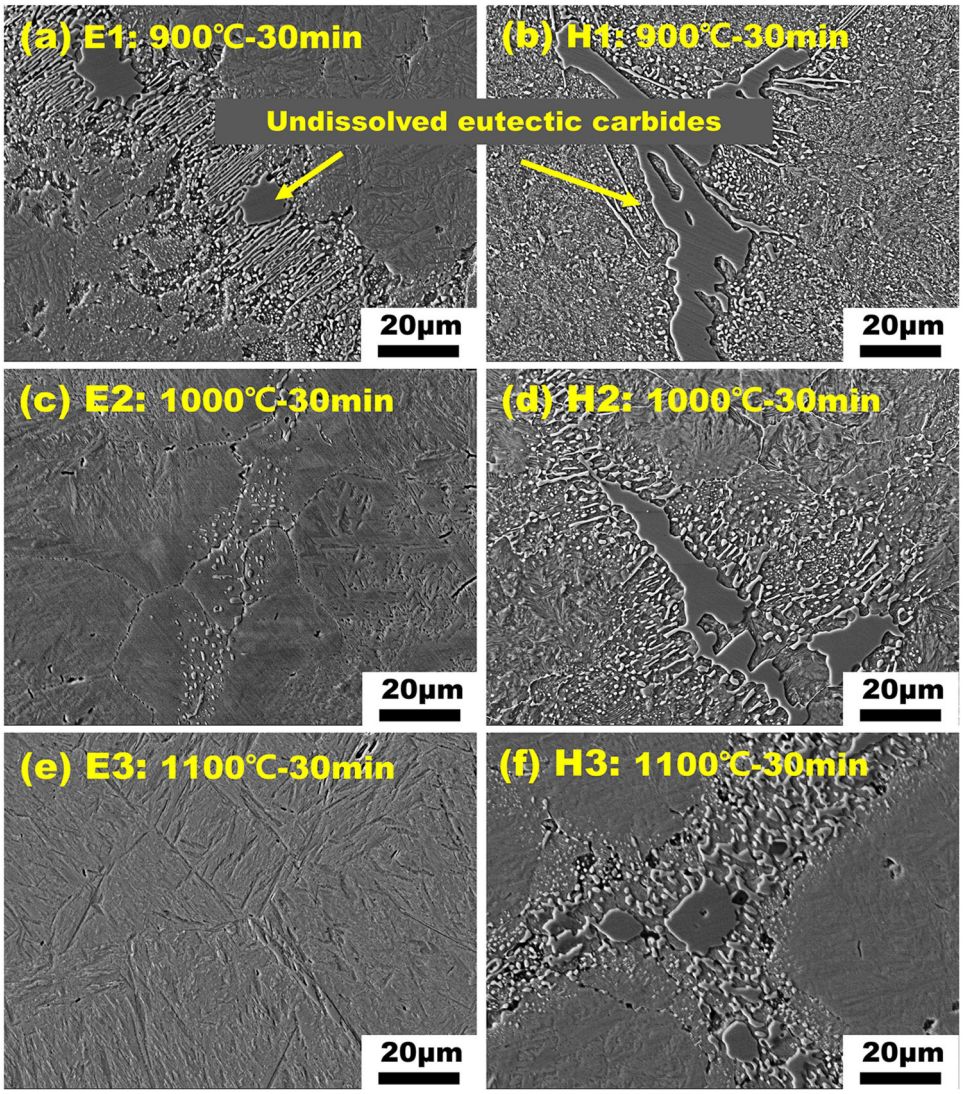

Fig. 3. SEM images of samples in different treatment states. Pulsed samples: (a) E1 900°C-30 min, (c) E2 1000°C-30 min, (e) E3 1100°C-30 min, (b, d, f) heat-treated samples under corresponding conditions.

gradually dissolved. To further verify this conclusion, thermodynamic calculation and a numerical model have been used to explain the dissolution behavior of the liquation carbide. In the current system, the potential obeys the Laplace equation and can be expressed as:[33]

$$\nabla^2\varphi(x,y) = \frac{\partial^2\varphi(x,y)}{\partial^2 x^2} + \frac{\partial^2\varphi(x,y)}{\partial^2 y^2} = 0 \qquad (2)$$

where $\varphi(x, y)$ is the potential at any position, and (x, y) is the abscissa and ordinate of the position, respectively. The current density $j(x, y)$ is determined by conductivity and microstructure and calculated by Ohm's rule:

$$j(x,y) = -\sigma(x,y)\cdot\nabla\varphi(x,y) \qquad (3)$$

The current distribution around the liquation carbide is calculated by Eq. 3, and the result is brought into Eq. 1 to calculate the electrical free energy. According to the microstructure of the original sample (Fig. 1), the liquation carbide is set as three closely arranged elliptical particles (Fig. 6a) in the model, and the dissolution process of the liquation carbide is simulated by adjusting the particle size and position (A: a = 17.5 μm, b = 3.5 μm; B: a = 15.5 μm, b = 3.0 μm; C: a = 10.0 μm, b = 2.0 μm; D: a = 7.5 μm, b = 1.0 μm; E: a = 5.0 μm, b = 0.5 μm). a and b represent the long-axis radius and the short-axis radius of the particle, respectively, and the distance between the center of the particles was 6 μm. The conductivity of the liquation carbide particles was set to 1.2×10^6 S/m, and the conductivity of the matrix was 3.3×10^6 S/m.[34] The potential of the system was 20 V, and the electric field size was 20 μm × 20 μm. The finite difference method and MatLab software were used to calculate the model.

Figure 6b, c, d, e, and f shows the current density distribution around the liquation carbide with

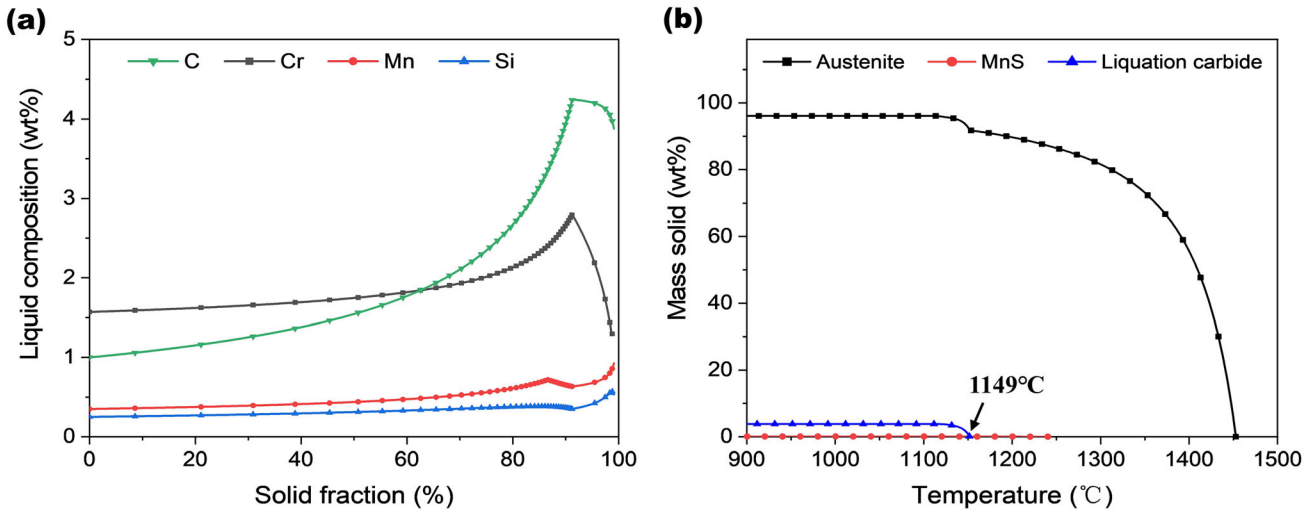

Fig. 4. Thermodynamic calculation results of the bearing steel solidification process: (a) change of element concentration in liquid phase, (b) precipitation behavior of phase.

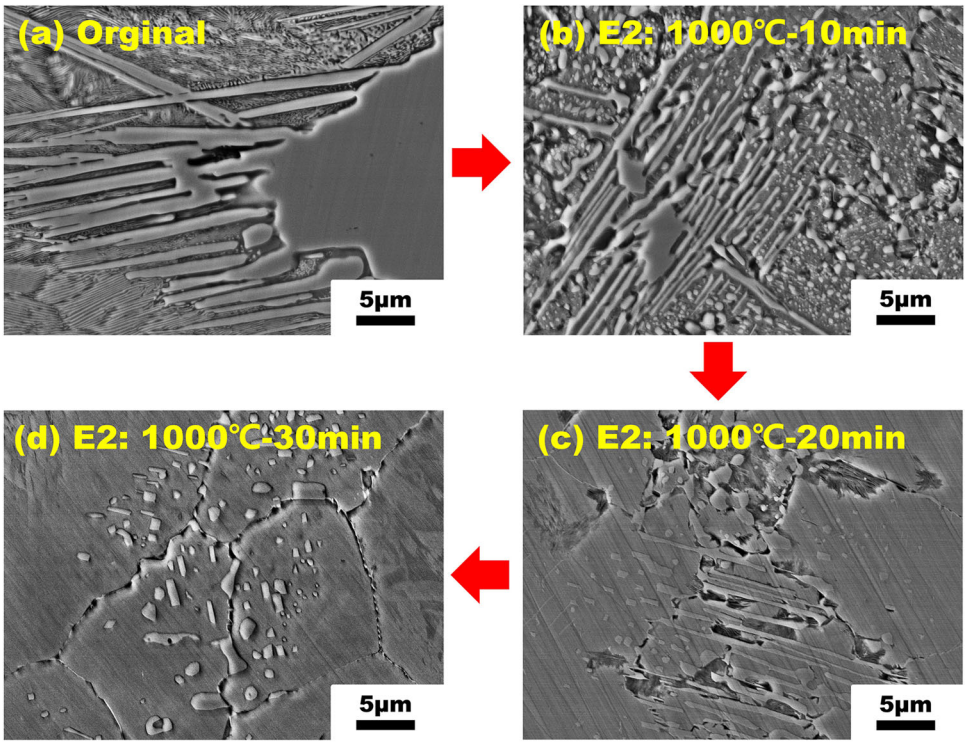

Fig. 5. The dissolution process of liquation carbide under pulsed electric current: (a) original state, (b) 1000°C-10 min, (c) 1000°C-20 min, (d) 1000°C-30 min.

different sizes, and Fig. 7 shows the relationship between the peak current density, the change of electrical free energy, and the change of carbide size. The electric field produces obvious distortion in the closely arranged gap of the liquation carbide lamellae due to the large curvature of the carbide tip, where the current density is significantly higher than that in other locations (Fig. 6b). The energy difference caused by the selective distribution of the current will promote the decomposition of massive liquation carbides along the gap. When reaching the critical state of dissolution (lamellar separation of liquation carbide), the degree of electric field distortion is the highest (Fig. 6c), and the maximum current density in the electric field reaches the peak (Fig. 7a). With the decrease of particle size, the lamellar spacing between particles gradually increases (the liquation carbide gradually dissolves), the electric field distortion caused by the liquation carbide gradually weakens (Fig. 6d, e, and

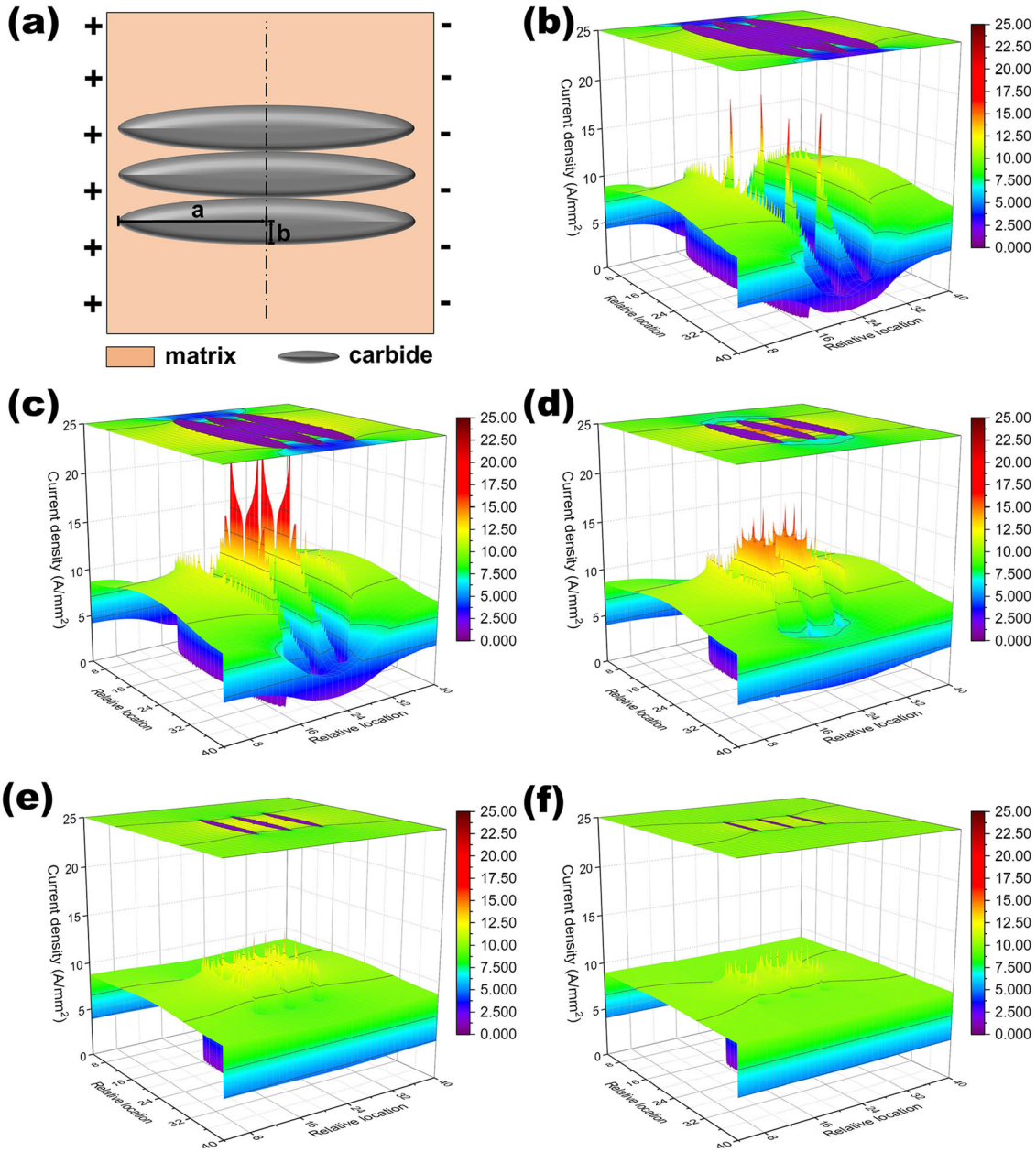

Fig. 6. Electric field model diagram and current density distribution calculation results: (a) schematic of the model. (b–f) calculation results of current distribution around the liquation carbide with different sizes (A: a = 17.5 μm, b = 3.5 μm; B: a = 15.5 μm, b = 3.0 μm; C: a = 10.0 μm, b = 2.0 μm; D: a = 7.5 μm, b = 1.0 μm; E: a = 5.0 μm, b = 0.5 μm). a and b represent the long-axis radius and the short-axis radius of the particle, respectively.

f), and the peak current density gradually decreases (Fig. 7a). Figure 7b shows the change of electrical free energy during the dissolution of the liquation carbides. With their gradual dissolution (particle size decreases and lamellar spacing increases), the change of electrical free energy rapidly decreases. Under the electric field, the material structure evolves toward the direction of reducing free energy, that is, the current promotes the dissolution of liquation carbide (high resistance phase), reduces the resistivity of the system, and finally obtains the system with lower free energy.[35,36]

Pulsed Electric Current Accelerating Atomic Diffusion to Eliminates the Segregation

The precipitation of the liquation carbide in the solidification structure is closely related to the dendrite segregation. The liquation carbide is precipitated at the last stage of solidification, and the degree of solute atom segregation in the liquation carbide region reaches the peak.[37] The fundamental purpose of the homogenization treatment is to make the elements in the material become evenly distributed, that is, to eliminate segregation.[38]

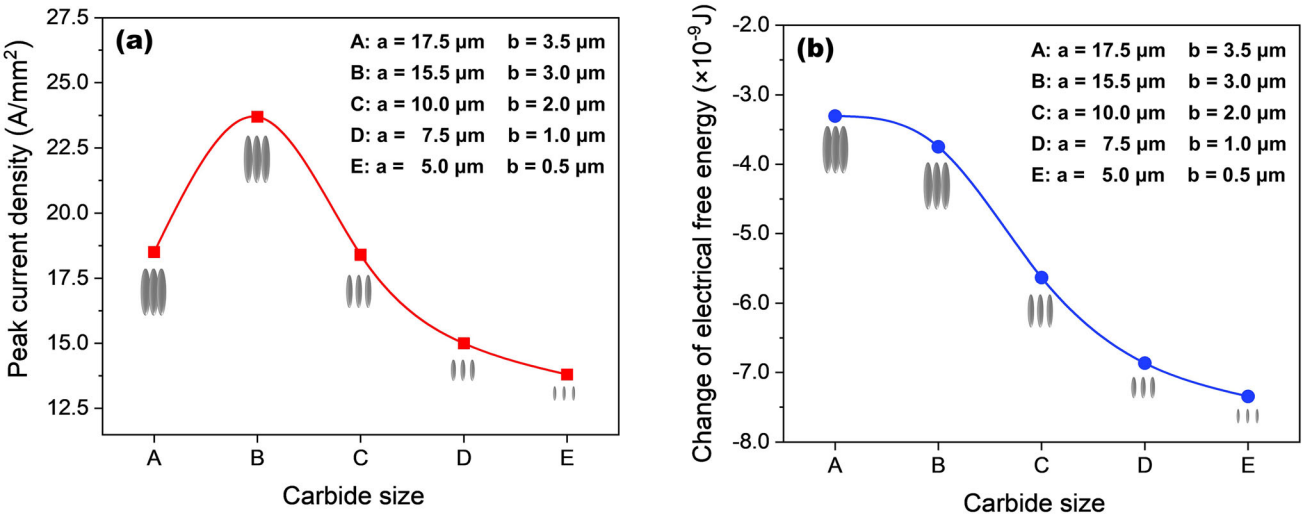

Fig. 7. Numerical calculation results of the dissolution process of liquation carbide: (a) the change of peak current density, (b) the change in electrical free energy.

Therefore, it is necessary to accurately analyze the element distribution in the samples by EPMA, and to evaluate the homogenization effect of the different treatment methods (pulsed electric current treatment and annealed treatment). The C and Cr elements are typical segregating elements in the solidification process of bearing steel, and they are also the main components of the liquation carbide. Meanwhile, the precipitation of the liquation carbide leads to the formation of an Fe-poor zone in this region. Therefore, EPMA was used to collect and analyze the distribution of the C, Cr, and Fe elements in the original sample (Y1), the industrial homogenized sample (G1), the pulsed sample (E3), and the annealed sample (H3). Compared with the original sample (Fig. 8a), the pulsed sample has a uniform distribution of the C, Cr and Fe elements (Fig. 8c). The homogenization effect of the short process pulsed treatment (30 min) is equivalent to that of the long process (300 min) industrial homogenization treatment (Fig. 8b). In addition, the distribution of the C, Cr and Fe elements in the annealed samples under the corresponding conditions is still very uneven, which indicates that dendritic segregation still exists (Fig. 8d).

The residual segregation coefficient is often used to characterize the homogenization effect:[39]

$$\delta_i = \frac{C^t_{max} - C^t_{min}}{C^0_{max} - C^0_{min}} = \exp\left(-\frac{4\pi^2}{L^2}Dt\right) \quad (4)$$

where C^0_{max} and C^0_{min} are the highest and lowest concentrations in the dendritic structure of the unprocessed ingot, respectively, C^t_{max} and C^t_{min} are the highest and lowest concentrations of the element i after homogenization, respectively, L is the distance between dendrites, t is the processing time, and D is the atomic diffusion coefficient. So, the smaller the residual segregation coefficient, the better the homogenization effect. The segregation of the Cr element in bearing steel is the most serious, and its distribution determines the whole homogenization process. In addition, C is difficult to be measured exactly by EPMA, so this study will use the Cr element as a representative to analyze the impact of the pulsed electric current on element diffusion. The quantitative distribution of the Cr element was measured by EPMA (Table II), and the diffusion coefficients of solute atom Cr in different treatment processes were calculated. According to Eq. 4, the diffusion coefficient, D, can change from the $\ln\delta$-t curve (Fig. 9). The corresponding slope values $-\frac{4\pi^2}{L^2}D$ obtained by fitting are -1.653×10^{-3} (E3: 1100°C), -4.053×10^{-5} (H3: 1100°C), and -1.572×10^{-4} (G1: 1220°C), and the corresponding diffusion coefficient has been calculated. In the pulsed sample (1100°C), the diffusion coefficient of the Cr atoms in the electric field was 2.36×10^{-13} m^2/s, while in the annealed sample (1100°C), the diffusion coefficient of the Cr atom in the thermal field was only 5.78×10^{-15} m^2/s. Compared to the thermal field, the diffusion coefficient of the Cr atoms in the electric field was about 40 times higher. In the industrial homogenized sample (1220°C), the diffusion coefficient of the Cr atom was 2.24×10^{-14} m^2/s, still lower than the calculated result in the electric field (2.36×10^{-13} m^2/s). Under the thermal field, the concentration gradient drives the diffusion of solute atoms, the liquation carbide slowly dissolves, and the degree of element segregation gradually decreases. At the same temperature, the pulsed electric current significantly improves the diffusion coefficient of the segregated atoms in the homogenization process, and the current significantly enhances the dissolution kinetics of the liquation carbides. Under the pulsed treatment, the solidification structure of the bearing steel will be homogenized more quickly.

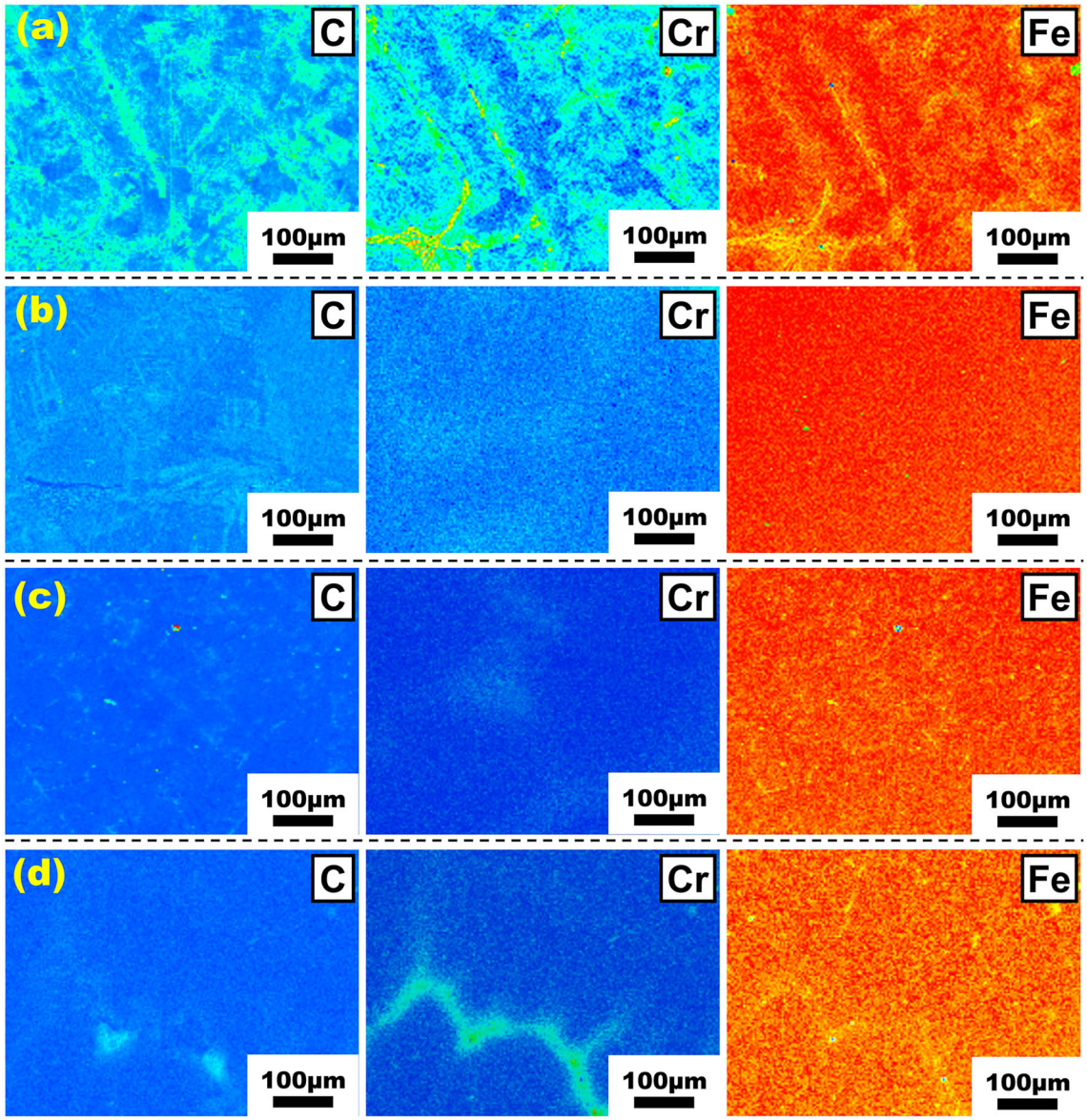

Fig. 8. EPMA area scanning results: (a) original sample (Y1), (b) industrial homogenized sample (G1: 1220°C-300 min), (c) pulse current-treated sample (E3: 1100°C-30 min, current density 19.4 A/mm^2), and (d) corresponding equivalent heat-treated sample (H3: 1100°C-30 min).

Table II. Residual segregation coefficient of Cr element

	E3 1100°C				H3 1100°C				G1 1220°C		
Time (min)	c^t_{max}	c^t_{min}	δ	Time (min)	c^t_{max}	c^t_{min}	δ	Time (min)	c^t_{max}	c^t_{min}	δ
10	11.84	1.06	0.98	10	11.84	1.06	0.98	100	5.21	1.22	0.36
20	11.66	1.13	0.95	20	11.66	1.13	0.95	200	2.80	1.36	0.13
30	11.51	1.24	0.93	30	11.51	1.24	0.93	300	2.05	1.53	0.05

The above results show that, compared with the traditional heat treatment, the pulsed electric current significantly accelerates the atomic diffusion rate to eliminate the segregation in a short time, and thus realizes the uniform distribution of the elements.

Grain Size Stability Under Pulsed Electric Current

The coarse grain structure in the slab will be inherited by the subsequent processing parts, which will deteriorate the strength of the material.

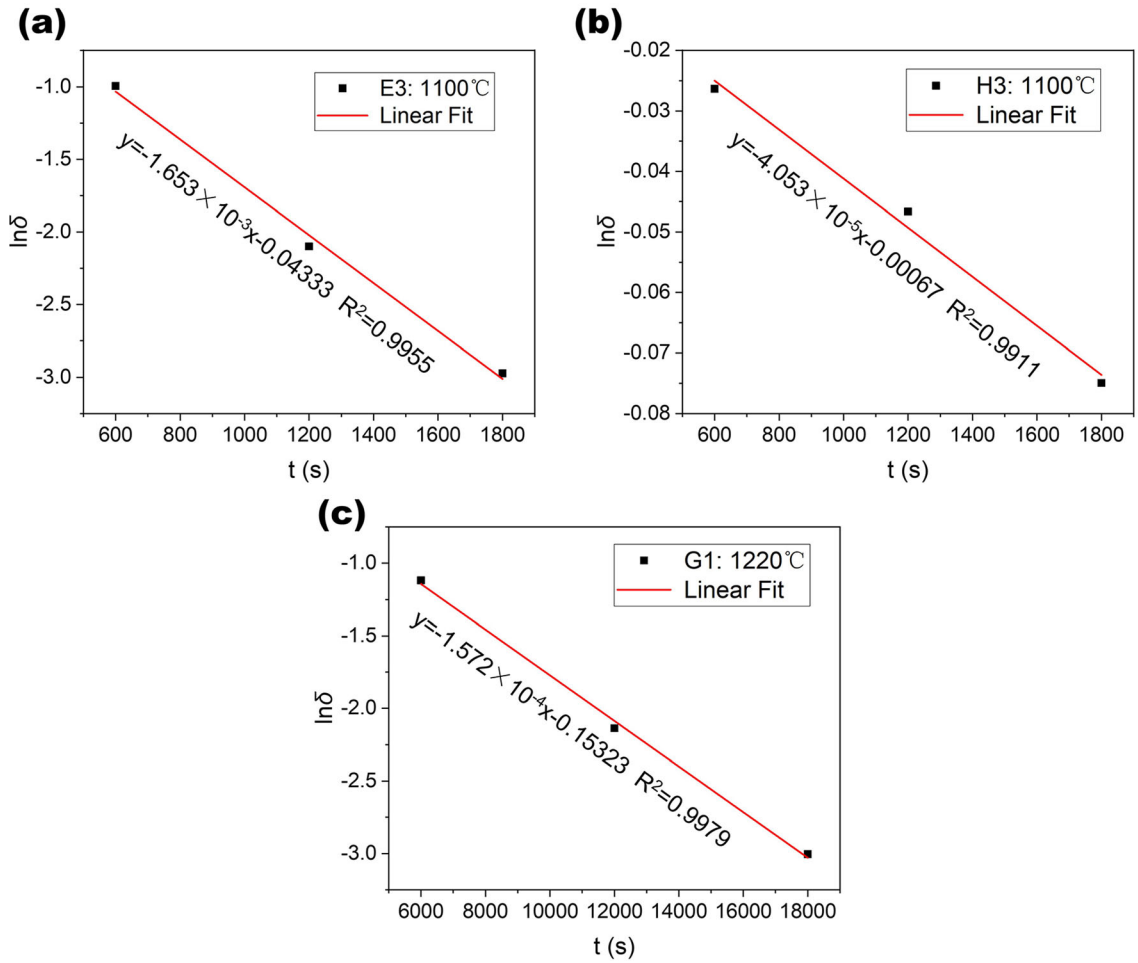

Fig. 9. lnδ–t linear relationship of the Cr element in different treatment processes: (a) pulsed treatment (E3: 1100°C-19.4 A/mm^2), (b) heat treatment (H3: 1100°C), (c) industrial homogenization treatment (G1: 1220°C).

Therefore, it is hoped to retain the fine grain structure in different processes. As mentioned above, pulse current treatment (E3: 1100°C-30 min) can effectively eliminate liquation carbide and dendrite segregation. The homogenization level of the pulsed sample is consistent with that of the industrial homogenized sample (G1: 1220°C-300 min). Pulsed treatment reduces the temperature required for homogenization and significantly shortens the treatment process. The change of homogenization conditions (temperature and time) will affect the grain size. As shown in Fig. 10a and b, there is a significant difference in the original austenite grain size between the pulsed sample and the industrial long process homogenized sample. In the pulsed sample, the grain size is concentrated at 200–600 μm and the average value is about 370 μm. However, in the industrial long process homogenized sample, the grain size is widely distributed at 800–3000 μm and the average value is about 1560 μm. Compared with the traditional long flow homogenization process, the pulsed treatment process can effectively avoid grain growth. This process not only ensures a good homogenization effect but also inhibits excessive grain growth, providing a good initial structure for subsequent hot deformation treatment (such as rolling and forging).

In this study, the pulsed treatment process (1100°C-30 min) and the industrial homogenization process (1220°C-300 min) have effectively eliminated the liquation carbide and dendrite segregation, and the alloy will obtain a single-phase austenite structure. After annealing, the grain size is proportional to the treatment time and inversely proportional to the treatment temperature.[40] The pulsed electric current treatment reduces the treatment temperature (from 1220°C to 1100°C) and significantly shortens the treatment time (from 300 min to 30 min), effectively inhibiting the grain growth during homogenization.

CONCLUSION

As-cast GCr15 bearing steel was taken as the research object, and the material homogenization was completed by using a pulsed electric current treatment instead of the traditional homogenization

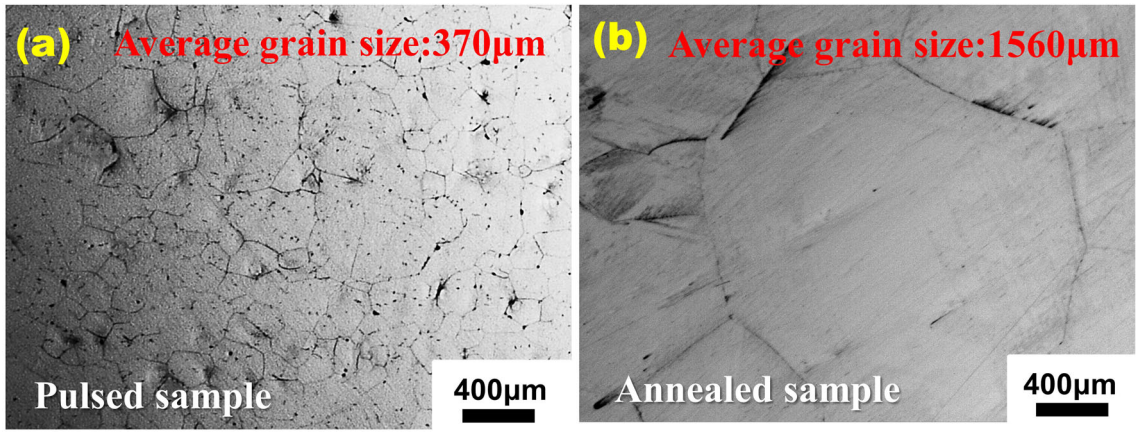

Fig. 10. Original austenite grain boundary and grain size distribution of samples in different treatment conditions: (a) pulsed sample (E3: 1100°C-30 min), (b) annealed sample (G1: 1220°C-300 min).

heat treatment. The pulsed samples and annealed samples were characterized by TEM, SEM, EPMA, and other equipment. Meanwhile, based on the electrical characteristics and morphology characteristics of the liquation carbide, the corresponding mathematical model was constructed, and the driving force of the pulsed electric current to eliminate the liquation carbide and dendritic segregation was analyzed from the thermodynamic and dynamic perspectives. The specific conclusions are as follows:

(1) In the pulsed sample (1100°C-30 min), the interdendritic liquation carbide and element segregation can be completely eliminated, and the homogenization effect is equivalent to that of the industrial high-temperature homogenization treatment (1220°C-300 min).
(2) In the process of the pulsed treatment, it is beneficial to maintain the stability of grain size due to the reduction of treatment temperature and treatment time, which provide a good initial structure for subsequent hot deformation treatment (such as rolling and forging), and high-strength products with fine grain structure. The average grain size of the pulsed sample was about 370 μm. However, the grain size of the industrial homogenization samples coarsened to 1560 μm due to long-term high-temperature retention.
(3) In the electric field, the current density at the gap of the liquation carbide layer is higher. The energy difference produced by the selective distribution of the current will promote the decomposition of the liquation carbide along the gap. The change of electrical free energy decreased with the size reduction, which is the driving force of the liquation carbide evolution.
(4) A pulsed electric current can significantly increase the diffusion coefficient of solute atoms, thereby rapidly realizing the homogenization of the bearing steel solidification structure.

ACKNOWLEDGEMENTS

The work was financially supported by the National Natural Science Foundation of China (U21B2082), Beijing Municipal Natural Science Foundation (2222065), and Fundamental Research Funds for the Central Universities (FRF-TP-22-02C2).

FUNDING

National Natural Science Foundation of China (Grant Numbers U21B2082, 51874023, U1860206, Beijing Municipal Natural Science Foundation (Grant Number 2222065), Nation Key Research and Development Program of China (Grant Number 2019YFC1908403, Fundamental Research Funds for the Central Universities (Grant Number FRF-TP-22-02C2).

DATA AVAILABILITY

The raw/processed data required to reproduce these findings cannot be shared at this time as the data also forms part of an ongoing study.

CONFLICT OF INTEREST

The authors declare that they have no known competing financial interests or personal relationships that could have appeared to influence the work reported in this paper.

REFERENCES

1. M. Woydt and R. Wäsche, *Wear* 268, 1542 (2010).
2. J.M. Beswick, *Montgomery: ASTM International* (2002).
3. N.K. Arakere, *Int. J. Fatigue* 93, 238 (2016).
4. H. Bhadeshia, *Prog. Mater. Sci.* 57, 268 (2012).
5. M. El Laithy, L. Wang, and T.J. Harvey, *Tribol. Int.* 140, 105849 (2019).
6. G. Krauss, *Metall. Mater. Trans. B* 34, 781 (2003).
7. S. He, C.S. Li, J.Y. Ren, and Y.H. Han, *Steel Res. Int.* 89, 1800148 (2018).
8. M. Reger, B. Vero, I. Felde, and I. Kardos, *J. Mech. Eng.* 56, 143 (2010).
9. S. Jiao, J. Penning, F. Leysen, Y. Houbaert, and E. Aernoudt, *ISIJ Int.* 40, 1035 (2000).

10. A. Costa e Silva, *J. Phase Equilib. Diff.* 41, 522 (2020).
11. S.K. Choudhary, S. Ganguly, A. Sengupta, and V. Sharma, *J. Mater. Process. Technol.* 243, 312 (2017).
12. N.Y. Du, H.H. Liu, Y.F. Cao, P.X. Fu, and D.Z. Li, *Mater. Charact.* 174, 111011 (2021).
13. K.H. Kim and C.M. Bae, *Met. Mater. Int.* 19, 371 (2013).
14. W.F. Liu, Y.F. Cao, Y.F. Guo, M.Y. Sun, B. Xu, and D.Z. Li, *J. Mater. Sci. Technol.* 38, 170 (2020).
15. A. Costa e Silva, *J. Phase Equilib. Diff.* 38, 916 (2017).
16. F.Y. Su, W.L. Liu, H. Wang, and W. Zhi, *Heat Transf.-Asian Re.* 49, 249 (2020).
17. F. Yu, X.P. Chen, H.F. Xu, H. Dong, Y.Q. Weng, and W.Q. Cao, *Acta Metall. Sin.-Engl.* 56, 513 (2020).
18. M. Michalec, P. Svoboda, I. Ktupka, and H. Martin, *Eng. Sci. Technol.* 24, 936 (2021).
19. X.F. Zhang and L.G. Yan, *Acta Metall. Sin.* 56, 257 (2020).
20. J.D. Guo, X.L. Wang, and W.B. Dai, *Mater. Sci. Technol.* 31, 1545 (2015).
21. R.S. Qin and A. Bhowmik, *Mater. Sci. Technol.* 31, 1560 (2015).
22. R. Landauer and J.W.F. Woo, *Phys. Rev. B* 10, 1266 (1974).
23. R. Ma, S.Q. Xiang, M.C. Zhou, and X.F. Zhang, *Mater. Sci. Eng. A* 843, 143131 (2022).
24. X.B. Liu, C.H. Liu, J.C. Wu, X.F. Zhang, X.R. Zhu, and J. Wang, *Mater. Sci. Eng. A* 832, 142421 (2022).
25. J.Q. Hao, S.Y. Qin, L.G. Yan, and X.F. Zhang, *J. Alloys Compd.* 873, 159854 (2021).
26. S.Y. Qin, J.Q. Hao, L.G. Yan, and X.F. Zhang, *Scr. Mater.* 199, 113879 (2021).
27. A.F. Khan, *Metals* 8, 800 (2018).
28. F. Hengerer, J. Beswick, and A. Kerrigan, *ASTM Spec. Tech. Publ.* 1195, 237 (1993).
29. V. Psyk, D. Risch, B.L. Kinsey, A.E. Tekkaya, and M. Kleiner, *J. Mater. Process. Technol.* 211, 787 (2011).
30. H.H. Ge, F.L. Ren, J. Li, X.J. Han, M.X. Xia, and J.G. Li, *Metall. Mater. Trans. A* 48, 1139 (2017).
31. X. Xuan, *Electrophoresis* 29, 33 (2008).
32. Y.B. Jiang, G.Y. Tang, C. Shek, Y.H. Zhu, and Z.H. Xu, *Acta Mater.* 57, 4797 (2009).
33. L.G. Yan, L. Chen, C.B. Liu, and X.F. Zhang, *Metall. Mater. Trans. B* 52, 1603 (2021).
34. U. Bohnenkamp, R. Sandstrom, and G. Grimvall, *J. Appl. Phys.* 92, 4402 (2002).
35. D. Leenov and A. Kolin, *J. Chem. Phys.* 22, 683 (1954).
36. Y. Dolinsky and T. Elperin, *Mater. Sci. Eng. A* 287, 219 (2000).
37. L.T. Gui, H. Zhang, Y. Zhao, Y.W. Wang, D.F. Chen, X.Y. Wang, G. Mahmud, and M.J. Long, *Materialia* 20, 101266 (2021).
38. P.D. Jablonski and J.K. Hawk, *J. Mater. Eng. Perform.* 26, 4 (2017).
39. X. Zhang, G.J. Ma, and M.K. Liu, *Philos. Mag.* 99, 1041 (2019).
40. K. Song and M. Aindow, *Mater. Sci. Eng. A* 479, 365 (2008).